Nuclear Materials and Energy 9 (2016) 194–198

Contents lists available at ScienceDirect

Nuclear Materials and Energy

journal homepage: www.elsevier.com/locate/nme

Experimental investigation of high He/dpa microstructural effects in neutron irradiated B-alloyed Eurofer97 steel by means of small angle neutron scattering (SANS) and electron microscopy

R. Coppola[a,*], M. Klimenkov[b], A. Möslang[b], R. Lindau[b], M. Valli[c]

[a] ENEA-Casaccia, FSN-SICNUC, Via Anguillarese 301, 00123 Roma, Italy
[b] KIT-IAM, PO Box 3640, D-76021 Karlsruhe, Germany
[c] ENEA-Faenza, SSTP-PROMAS-TEMAF, Via Ravegnana 186, 48018 Faenza (RA), Italy

ARTICLE INFO

Keywords:
Helium effects
Neutron irradiation
Small angle neutron scattering
Electron microscopy

ABSTRACT

High He/dpa microstructural effects have been investigated, by means of small-angle neutron scattering (SANS) and transmission electron microscopy (TEM), in B-alloyed ferritic/martensitic steel Eurofer97-1 (0.12 C, 9 Cr, 0.2 V, 1.08 W wt%, B contents variable between 10 and 1000 ppm), neutron irradiated at the High Flux Reactor of the JRC-Petten at temperatures between 250 °C and 450 °C, up do a dose level of 16 dpa. Under these irradiation parameters, B activation is expected to produce corresponding helium contents variable between 80 and 5600 appm, with helium bubble distributions relevant for the technological applications. The SANS measurements were carried out under magnetic field to separate nuclear and magnetic SANS components; a reference, un-irradiated sample was also measured to evaluate as accurately as possible the genuine effect of the irradiation on the microstructure. Increasing the estimated helium content from 400 to 5600 appm, the analysis of the SANS cross-sections yields an increase in the volume fraction, attributed to helium bubbles, of almost one order of magnitude (from 0.007 to 0.038); furthermore, the difference between nuclear and magnetic SANS components is strongly reduced. These results are discussed in correlation with TEM observations of the same samples and are tentatively attributed to the effect of drastic microstructural changes in Eurofer97-1 for high He/dpa ratio values, possibly relating to the dissolution of large B-carbides due to transmutation reactions.

1. Introduction

This study concerns the ferritic/martensitic steel Eurofer97-1 (0.12 C, 9 Cr, 0.2 V, 1.08 W wt%), a European reference for fusion-related studies. The original composition, reported here above, has been modified introducing, by alloying, natural B contents variable between 10 and 1000 ppm in order to produce, under neutron irradiation and consequent B activation, corresponding helium contents and helium bubble distributions relevant for the technological applications. Such B-alloyed Eurofer97-1 heats have been neutron irradiated at the High Flux Reactor of the JRC-Petten, at temperatures between 250 °C and 450 °C, up do a dose level of 16 dpa. Reference is made to [1–7] for results of post-irradiation mechanical testing and transmission electron microscopy (TEM) observations of these samples. SANS results on B-alloyed Eurofer97-1 up to 400 appm helium content have been published in ref.s [8–10] and are reported in this paper for quantitative comparison with the new SANS results, obtained on B-alloyed Eurofer97-1 with 5600 appm helium content. As it is discussed in refs. [1–7], the microstructural changes produced under neutron irradiation in these B-alloyed heats are very representative of the working conditions in a *tokamak*, due to the high He/dpa ratio; on the other hand, their characterization is quite complex because of the simultaneous production of helium bubbles and micro-voids, in addition to possible changes in precipitate density and composition. Complementary techniques, like TEM and SANS, are therefore indispensable to characterize all these effects, correlate them with post-irradiation mechanical testing results and finally contribute to predict the behavior of this steel under service conditions.

* Corresponding author.
E-mail address: roberto.coppola@enea.it (R. Coppola).

http://dx.doi.org/10.1016/j.nme.2016.09.013

2. Material characterization

The investigated material is Eurofer97-1 (0.12 C, 9 Cr, 0.2 V, 1.08 W Fe bal wt%) modified introducing, by alloying, a B-10 content of 0.0083 mass-% (ADS3 heat) and of 0.1120 mass-% (ADS4 heat), corresponding respectively to estimated helium concentrations of 400 appm and 5600 appm under neutron irradiation; these heats were originally developed also for studies relating to Accelerator Driven System. The samples had been neutron irradiated at the High Flux Reactor of the JRC-Petten at 400 °C/450 °C to a dose level of 16 dpa. The SANS results presented in this paper refer to two B-alloyed Eurofer97-1 heats, one irradiated to 16 dpa at 450 °C with expected helium concentration of 400 appm (ADS3 heat), the other irradiated to 16 dpa at 400 °C with expected helium concentration of 5600 appm (ADS4 heat); for each of these two irradiated samples a corresponding reference, un-irradiated one was measured. All these samples were obtained from heats submitted to the preliminary standardization treatment (1040 °C 30′ + 760 °C 1.5 h).

The irradiated samples were obtained as platelets, approximately $4 \times 9\,mm^2$ in surface and 1 mm thick, cutting them from the KLST specimens prepared for post-irradiation mechanical testing [1]. The reference, un-irradiated samples were $1\,cm^2$ in surface and 1 mm thick; the microstructural effect of ageing at 450 °C was experimentally checked up to 500 h, finding no changes in the SANS cross-section [10].

TEM observations of $M_{23}C_6$ and MX precipitates both in these heats before irradiation and in un-irradiated Eurofer97-1 are shown in ref.s [6,11] respectively. No significant changes in density or composition of such carbide precipitates was detected by TEM in the irradiated B-alloyed Eurofer 97–1 [4–7] and no occurrence of dislocation loops and other structural radiation induced defects was observed. Furthermore, in these ADS heats, before irradiation, locally inhomogeneous B distributions were observed, together with BN and $M_{23}(C,B)_6$ precipitates, as large as a few μm [6]. After irradiation, in correspondence of the former B-precipitates, He/Li rich halos with empty spaces in the central parts were locally observed as a consequence of the B disappearance due to the transmutation reactions, particularly for 5600 helium appm [4].

Nano-sized helium bubbles appear by far as the dominant microstructural feature detected by TEM in these irradiated B-alloyed Eurofer97-1 samples: typical pictures are shown in Fig. 1(a and b) [7]. For the material with 400 appm helium (Fig. 1a) the bubbles are inhomogeneously distributed inside, often concentrated on former dislocation lines or grain boundaries; their shape appears often cuboidal. Much larger bubble sizes are detected in material with 5600 appm helium (Fig. 1b). The corresponding size histograms of the bubbles are shown in Section 4 together with the SANS distributions. It is noted that the TEM resolution power decreases strongly for sizes below 10 Å and that it is not easy to distinguish by this technique helium bubbles and micro-voids for the reasons discussed in ref. [7]. Fig. 1c shows a typical halo, surrounding an empty region originated by B-precipitate dissolution (from ref. [4]).

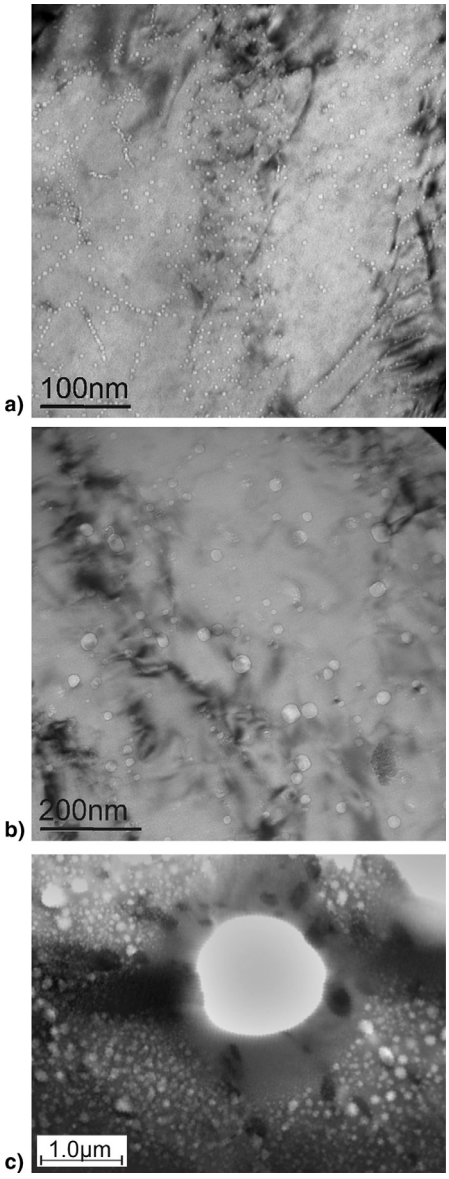

Fig. 1. TEM pictures of helium bubbles in B-alloyed Eurofer97-1 steel, neutron irradiated at 400 °C/450 °C 16 dpa for estimated helium contents 400 appm (a) and 5600 appm (b) [7].]. A typical "halo", surrounding an empty region originated by B-precipitate dissolution in ADS4 heat (5600 helium appm), is shown in c) from ref. [4].

3. Experimental technique and results

General information on SANS can be found in ref.s [12,13], in previous works on Eurofer97-1 [8–10,14–16] and in another contribution to these proceedings [17]. Defining the modulus of the scattering vector $Q = 4\pi \sin\theta/\lambda$ (where 2θ is the full scattering angle and λ the neutron wavelength), for magnetic samples, applying an external magnetic field to saturate the magnetization in the matrix, the total SANS cross-section $d\Sigma(Q)/d\Omega$ (where Ω stands for the solid angle) can be written as the sum of two terms, a nuclear and a magnetic one

$$d\Sigma(Q)/d\Omega = d\Sigma(Q)/d\Omega_{nucl} + d\Sigma(Q)/d\Omega_{mag} \sin^2\alpha \quad (1)$$

where α is the azimutal angle on the detector plane with respect to the applied magnetic field. The ratio $R(Q)$ (also defined as "A" in the scientific literature) of the SANS components perpendicular and parallel to this field

$$R(Q) = \frac{d\Sigma(Q)/d\Omega_{nucl} + d\Sigma(Q)/d\Omega_{mag}}{d\Sigma(Q)/d\Omega_{nucl}} = 1 + (\Delta\rho)^2_{mag}/(\Delta\rho)^2_{nucl} \quad (2)$$

is related to the composition of the microstructural inhomogeneities, $(\Delta\rho)^2$ being the "contrast" or square difference in neutron scattering length density (nuclear and magnetic respectively) between the observed nuclear and magnetic inhomogeneities and the matrix [12,13]. Dependence on Q implies that defects of different composition for different sizes are present in the investigated

sample (in this case Eq. (2) has to be modified to account for their combination). In the case of Eurofer97-1, assuming that the carbide precipitate composition is $Cr_{14}Fe_8W_{0.7}V_{0.3}C_6$ [11] a contrast value of 2.13 10^{20} cm^{-4} is found; for the case of micro-voids the nuclear contrast is equal to the squared scattering length density of Eurofer97-1 itself, that is 5.51 10^{21} cm^{-4}, while for the case of helium bubbles it is 4.88 10^{21} cm^{-4}. Therefore, both helium bubbles and micro-voids are expected to give rise to SANS effects one order of magnitude larger than precipitates (for comparable densities) but are quite difficult to be distinguished from one another. It is noted that non-magnetic precipitates, like $M_{23}C_6$, behave as magnetic holes in the fully magnetized Eurofer97-1 matrix; consequently they can significantly contribute in the magnetic SANS component, provided their volume fraction is at least comparable to the one of helium bubbles or micro-voids.

If the volume fraction of the investigated inhomogeneities is low, with no inter-particle interference, the SANS nuclear and magnetic cross-sections can each one be written as

$$d\Sigma(Q)/d\Omega = (\Delta\rho)^2 \int_0^\infty dR\, N(R)\, V^2(R)\, |F(Q,R)|^2 \qquad (3)$$

where $N(R)$ is the number per unit volume of defects with a size between R and $R+dR$, V their volume and $|F(Q,R)|^2$ their form factor (assumed spherical in this case). The volume distribution function is defined as:

$$D(R) = N(R)R^3 \qquad (4)$$

$N(R)$ was determined, by transformation of Eq. (3), using the method described in [18,19]. In the case of large helium bubbles, Eq. (3) has to be adapted by introducing the contrast dependence on the bubble radius [20,23]; for small bubbles such correction produces negligible effects on the final result of the best-fit and turns out to be smaller than the statistical error band associated to the fitting procedure [22].

The SANS measurements were carried out at the D22 instrument at the High Flux Reactor of the Institut Max von Laue - Paul Langevin (ILL), Grenoble. The two irradiated samples had to be transported to the neutron source in different times and included in two separate SANS experiment. The sample containing 400 appm helium and its un-irradiated reference were measured with $\lambda = 6$ Å and sample-to-detector distances of 2 m and 11 m, covering a Q-interval ranging from 3 10^{-3} $Å^{-1}$ to 2.6 10^{-1} $Å^{-1}$ (sizes $2R \sim \pi/Q$ varying between 10 Å and 1000 Å approximately). The sample containing 5600 appm helium and its un-irradiated reference were measured with $\lambda = 6$ Å and sample-to-detector distances of 3.5 m and 11.2 m (Q interval ranging from 2 10^{-3} $Å^{-1}$ to 0.16 $Å^{-1}$, particle sizes ranging from 20 Å to 1500 Å approximately); for technical reasons, shorter counting times had to be selected during this experiment. In both experiments, an external 1 T magnetic field was applied and the same reference, un-irradiated Eurofer97-1 sample (ADS3) was additionally measured for a check; calibration to absolute SANS cross-section was obtained by the ILL standard programs. Within the experimental uncertainties, no SANS difference was detected between the un-irradiated references ADS3 and ADS4 measured in the two different experiments [10]. The experimental errors on the data reported in Fig. 3 are generally below 3%.

Fig. 2a and b show the 2D SANS patterns of the investigated samples: increasing the nominal helium concentration from 400 appm to 5600 appm results in a consistent increase of the neutron counts and, additionally, in a strong reduction of the magnetic anisotropy SANS component (together with the $R(Q)$ ratio). Fig. 3a and b show the SANS nuclear cross-section and $R(Q)$ values of irradiated samples ADS3 (450 °C 16 dpa 400 appm helium) [8,9], ADS4 (400 °C 16 dpa 5600 appm helium) and of the un-irradiated ADS3 reference. As already discussed in [8,9], Fig. 3 shows that for

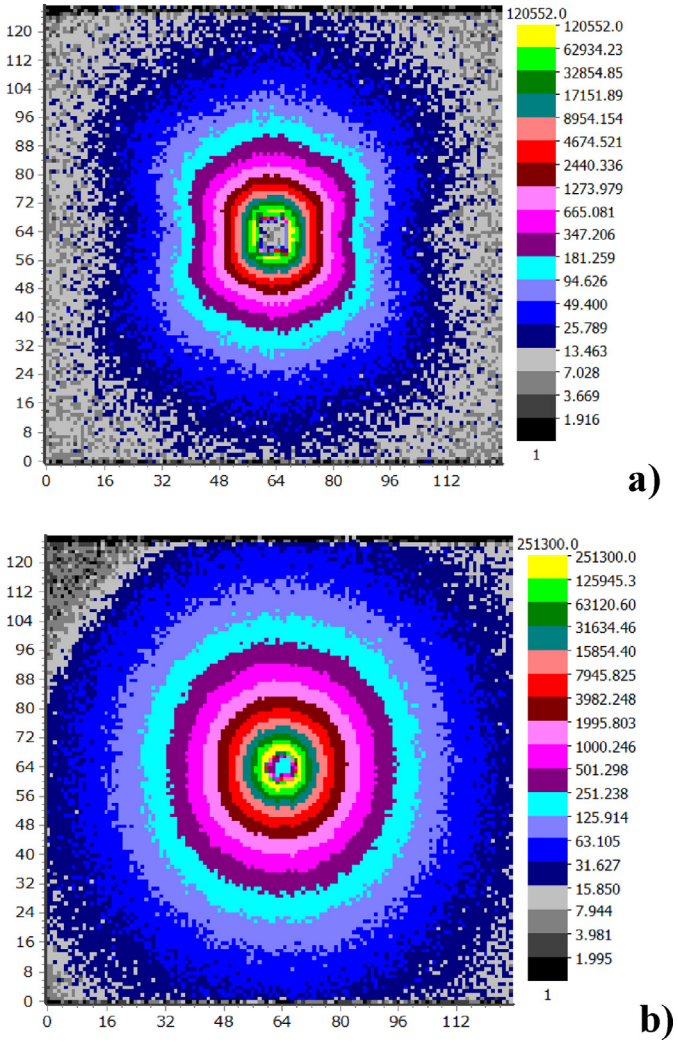

Fig. 2. 2D SANS patterns (neutron counts) for the Eurofer97-1 ADS3 irradiated at 450 °C to 16 dpa 400 appm helium (a) and ADS4 irradiated at 400 °C to 16 dpa 5600 appm helium (b); the direction of the external magnetic field is horizontal in the plane of the figure.

400 appm helium content the effect of the irradiation on the SANS cross-section is detected for 3 10^{-2} $Å^{-1} < Q < 2.6$ 10^{-1} $Å^{-1}$, corresponding to defect sizes smaller than 100 Å approximately.

For $Q < 3$ 10^{-2} $Å^{-1}$ there is almost no detectable difference between reference and irradiated samples, both following a "Porod behavior" (Q^{-4} cross-section dependence on Q) [11,12]: this is attributed to the distributions of very large carbide precipitates ($R > 500$ Å) characterized by TEM in standard Eurofer97, both un-irradiated and after neutron irradiation [24]. When the helium concentration is increased to 5600 appm, the SANS cross-section increases by one order of magnitude over all the investigated Q interval, reflecting the occurrence of a high density of broadly distributed inhomogeneities. Fig. 3b shows that the $R(Q)$ ratio is strongly Q-dependent for the un-irradiated reference, with values compatible with the presence of carbides [8,9]. For 400 appm helium it approaches the value of 2, corresponding to non-magnetic defects embedded in a fully magnetized matrix (Eq. (2)). For 5600 appm it is close to 1.3, implying a consistently lower value for the magnetic contrast.

The volume distribution functions have been determined for the two irradiated samples from the SANS data shown in Fig. 3. As explained in ref.s [22,23], in the case of a polydisperse system, like the investigated samples, these distributions, rather than the $N(R)$,

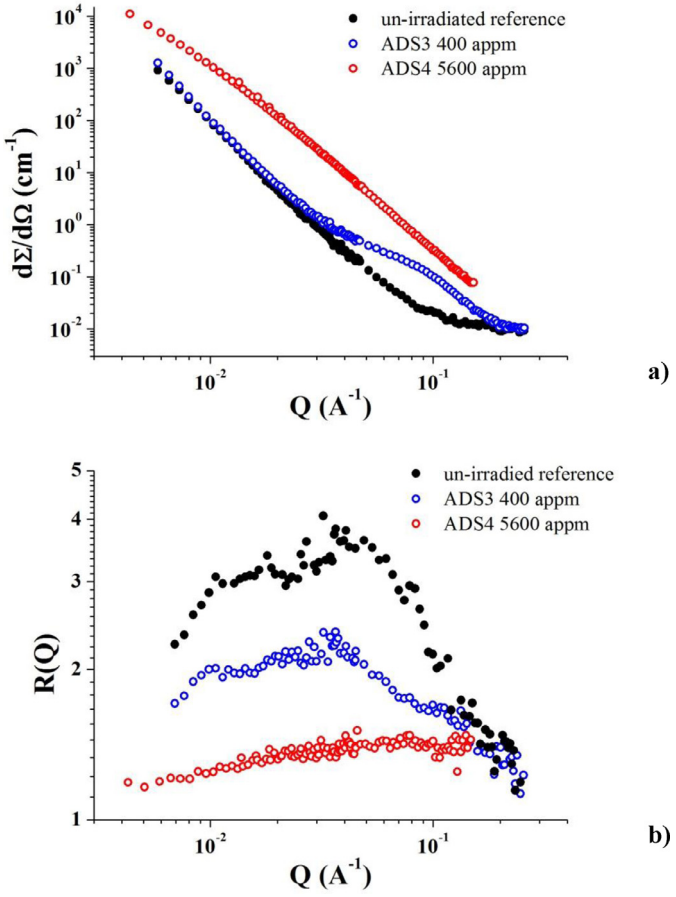

Fig. 3. SANS nuclear cross-section (a) and *R(Q)* (b) for the Eurofer97-1 ADS3 un-irradiated reference (black), ADS3 irradiated at 450 °C to 16 dpa 400 appm helium (blue) [8,9], and ADS4 irradiated at 400 °C to 16 dpa 5600 appm helium (red). (For interpretation of the references to colour in this figure legend, the reader is referred to the web version of this article.)

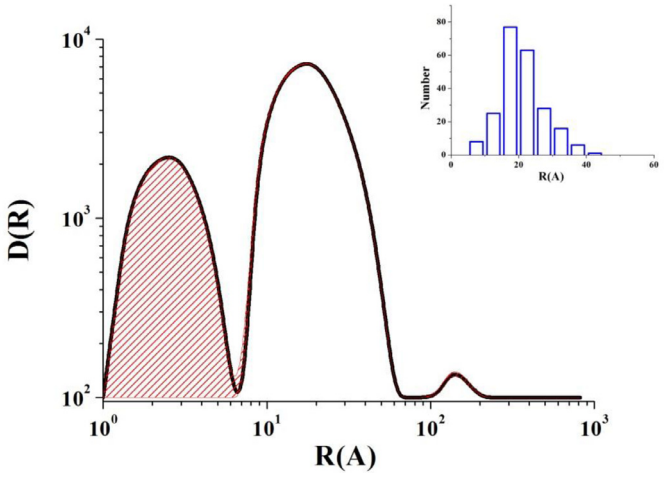

Fig. 4. Eurofer 97–1 ADS3 irradiated at 450 °C to 16 dpa 400 appm helium, volume distribution in $Å^{-1}$ [8, 9] with 80% confidence band (dashed area), and TEM histogram [7] in the insert; both are attributed to helium bubbles.

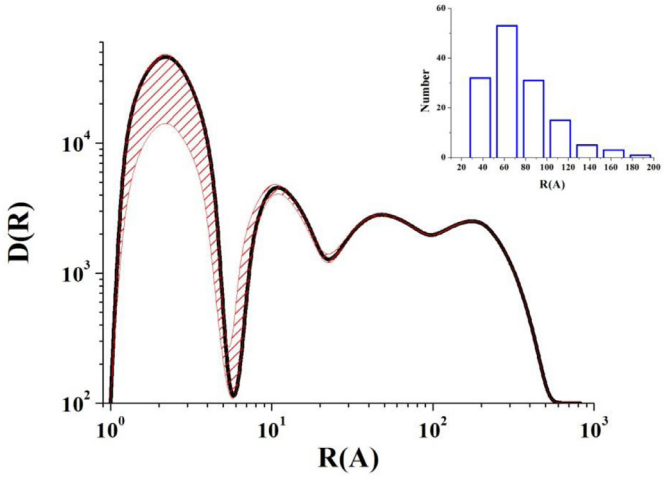

Fig. 5. Eurofer 97–1 ADS4 irradiated at 400 °C to 16 dpa 5600 appm helium, volume distribution in $Å^{-1}$ with 80% confidence band (dashed area), and TEM histogram [7] in the insert; both are attributed to helium bubbles.

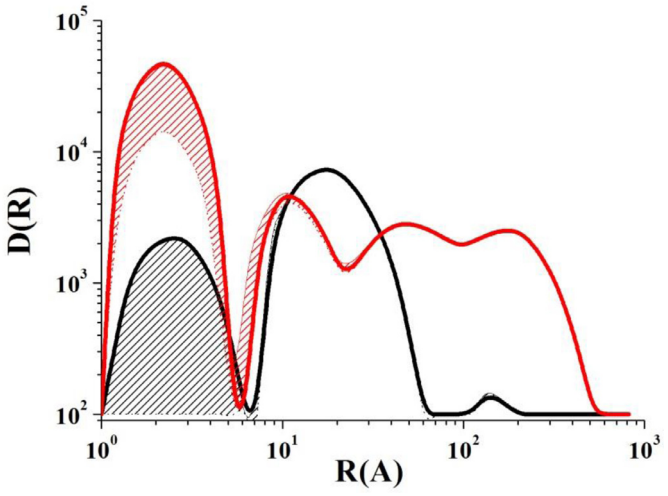

Fig. 6. Volume distribution functions ($Å^{-1}$), with 80% confidence band (dashed area), attributed to helium bubbles obtained from SANS nuclear cross-sections of B-alloyed Eurofer97-1 5600 appm helium neutron irradiated at 400 °C to 16 dpa (red) and 400 appm helium neutron irradiated at 450 °C to 16 dpa (black). (For interpretation of the references to colour in this figure legend, the reader is referred to the web version of this article.)

are more meaningfully compared with the TEM histograms, taking also into account that the observed SANS effects are weighted with the square volume of the scattering inhomogeneities (Eq. (3)).

In the case of 400 appm helium, the reference, un-irradiated sample was subtracted from the irradiated one and the distribution determined excluding the "Porod" region from the transformation procedure, as described in [8,9]: in fact, for such small Q-values the SANS effects is attributed mostly to large carbide precipitates, nearly un-changed before and after irradiation (Section 2). In the case of 5600 appm helium, the subtraction of the un-irradiated reference has no significant influence on the distribution of the irradiated one, since it constitutes an almost negligible background (Fig. 3); the transformation procedure has been applied to the whole investigated *Q* range, obtaining a good fit. It was assumed that, in both samples, the observed SANS effects are mostly due to helium bubbles; as a first approximation, the contrast dependence on bubble radius for the larger bubbles (typically $R > 100$ Å) [20–22] has not been included in the fitting procedure. The volume distribution the irradiated ADS3 sample containing 400 appm is shown in Fig. 4 together with the TEM histogram obtained on the same material and attributed to helium bubbles [7]; an estimated helium bubble volume fraction of 0.007 is obtained. For the irradiated ADS4 sample containing 5600 appm helium, the volume distribution is shown in Fig. 5, together with the TEM histogram obtained on the same material and attributed to helium bubbles [7]; an estimated helium bubble volume fraction of 0.038 is ob-

tained. Fig. 6 shows a comparison between the volume distributions obtained for the two irradiated samples.

4. Discussion and conclusions

The results presented in Figs. 2 and 3 show that increasing from 400 appm to 5600 appm the expected helium concentration, produced in Eurofer97 under neutron irradiation via B activation, an increase of roughly one order of magnitude in the SANS cross-section is observed, together with a strong reduction of the magnetic SANS component and *R(Q)* ratio. For nuclear neutron "contrast" reasons and based on TEM observations of these same samples, the increase in nuclear SANS cross-section is primarily attributed to helium bubbles or to micro-voids, which are however difficult to distinguish both by SANS and by TEM. Under this assumption, anyhow, the obtained helium bubble volume fractions of 0.007 and of 0.038, respectively for 400 appm and 5600 appm helium contents, are consistent with the irradiation conditions. The qualitative agreement between SANS obtained volume distributions and TEM histograms (Figs. 4 and 5) is satisfactory, taking also into account that volumes several orders of magnitude larger are sampled by SANS and that the statistics attainable by even very accurate TEM observation is further limited by the difficulty of thinning the samples without modifying the distribution of micro-voids and helium bubbles. Work is underway to quantitatively compare the volume fractions, attributed to the helium bubbles, determined by SANS and by TEM, taking into account possible truncation effects in the TEM histograms for very large bubbles (Fig. 5), depending on poor statistics and possible destruction of such large bubbles during thinning. Furthermore, increasing of one order of magnitude the helium concentration, produced via B transmutations, the SANS measurements show a reduction of the magnetic SANS component, certainly related to deep microstructural changes the B-alloyed Eurofer97-1. An almost non-magnetic behavior of the matrix would be compatible with Eq. (2) and the measured value of the *R(Q)* ratio (Fig. 3b). It could possibly be explained by a significant density of large-scale inhomogeneities originated by the dissolution of B precipitates, like the one shown in Fig. 1c. Provided their volume fraction is sufficiently high, such non-magnetic and large (up to 10 μm) inhomogeneties would contribute to SANS well outside the selected experimental window, but could reduce the effective average magnetic scattering length density of the matrix: however, based on the statistics of the currently available TEM observations, this can only be suggested as a possible explanation to be further experimentally investigated. SANS measurements extended to much smaller *Q* values than the available ones as well as high-angle diffraction measurements (to check the occurrence of structural changes) will be very useful; magnetization measurement of the irradiated sample could also be useful. Work is underway to complete the investigation of these and other irradiated samples with 5600 appm helium [25] by means of polarized SANS measurements and for different values of the external magnetic field, in order to obtain additional information useful to quantitatively characterize the SANS contribution originating from the helium bubbles and to understand the magnetic changes observed for higher B contents.

Acknowledgments

This work, supported by the European Commission under the contract of Associations, was carried out within the framework of the European Fusion Development Agreement. The views and opinions expressed herein do not necessarily reflect those of the European Commission.

References

[1] E. Materna-Morris, A. Möslang, S. Baumgärtner, J. Ehrmann, E. Gaganidze, M. Holzer, S. Lautensack, H. Ries, R. Rolli, H.-C- Schneider, H. Zimmermann, FZK Rep. IMF I No. 092 FUSION N0323, Dec. 2008
[2] E. Materna-Morris, A. Möslang, R. Rolli, H.-C. Schneider, J. Nucl. Mat 386-388 (2009) 422–425.
[3] M. Klimenkov, P. Vladimirov, A. Möslang, E. Materna-Morris, H.-C. Schneider, Int. J. Mat. Res. 102 (2011) 9.
[4] M. Klimenkov, A. Möslang, E. Materna-Morris, H.-C. Schneider, J. Nucl. Mat 442 (2013) S52–S57.
[5] M. Klimenkov, A. Möslang, E. Materna-Morris, Micron 46 (2013) 51–56.
[6] E. Materna-Morris, M. Klimenkov, A. Möslang, Mat. Sc. For. 730-732 (2013) 877–882.
[7] M. Klimenkov, A. Möslang, E. Materna-Morris, J. Nucl. Mat. 453 (2014) 54–59.
[8] R. Coppola, M. Klimenkov, R. Lindau, L. Porcar, M. Sepielli, M. Valli, in: Duncan J. McGillivray, Jill Trewhella, Elliot P. Gilbert, Tracey L. Hanley (Eds.), Proceedings of the 15th International Small-Angle Scattering Conference, 2012 ISBN 1 921.
[9] R. Coppola, M. Klimenkov, R. Lindau, B.R. Pauw, M. Valli, *Defect Distributions in Irradiated Nuclear Steels as Investigated with Complementary TEM and Small-Angle Neutron Scattering* oral presentation at the EMMM 2013 Conference, 2013 November.
[10] R. Coppola, M. Valli, EFDA Report for MAT-IREMEV – Task Agreement 2012, Task WP12_MAT_01_IREMEV_05_02/ENEA_Frascati/PS, Jan. 2013
[11] M. Klimenkov, R. Lindau, E. Materna-Morris, A. Möslang, Prog. Nuc. En. 57 (2013) 8–13.
[12] G. Kostorz, X-ray and neutron scattering, in: R.W. Cahn, P. Haasen (Eds.), Physical Metallurgy, North Holland, 1983, pp. 793–853.
[13] M.T. Hutchings, C.G. Windsor, in: K. Sköld, D.L. Price (Eds.), Methods of Experimental Physics, vol 23-c, Neutron Scattering, Academic, 1987, pp. 405–482.
[14] R. Coppola, R. Lindau, M. Magnani, R.P. May, A. Möslang, J.W. Rensman, B. van der Schaaf, M. Valli, F. Eng. Des. 75-79 (2005) 985–988.
[15] R. Coppola, R. Lindau, R.P. May, A. Möslang, M. Valli, J. Nuc. Mat 386-388 (2009) 195–198.
[16] R. Coppola, M. Klimenkov, R. Lindau, A. Möslang, M. Valli, A. Wiedenmann, J. Nuc. Mat. 409 (2011) 100–105.
[17] R. Coppola, C. Dethloff, E. Gaganidze, R. Lindau, M. Valli, J. Aktaa, A. Möslang, NME (2016) in print.
[18] M. Magnani, P. Puliti, M. Stefanon, Inst. Meth. A 217 (1988) 611–616.
[19] R. Coppola, R. Kampmann, M. Magnani, P. Staron, Acta Mat. 46 (1998) 5547-5456.
[20] Qiang-Li, W. Kesternich, H. Schroeder, D. Schwahn, H. Ullmaier, Acta Met. Mat. 38 (1990) 2383–2392.
[21] G. Albertini, F. Carsughi, R. Coppola, W. Kesternich, F. Rustichelli, G. Mercurio, D. Schwahn, H. Ullmaier, J. Nuc. Mat. 191-194 (1992) 132–137.
[22] R. Coppola, M. Klimiankou, R. Lindau, A. Möslang, M. Valli, J. Nuc. Mat. 329-333 (2004) 1057–1061.
[23]) R. Coppola, M. Klimenkov, R. Lindau, A. Möslang, M. Valli, A. Wiedenmann, J. Nuc. Mat. 409 (2011) 100–105.
[24] C. Dethloff, E. Gaganidze, J. Aktaa, J. Nuc. Mat. 454 (2014) 323–331.
[25] Work in preparation by the same authors.